Renewable Energy 51 (2013) 302–309

Contents lists available at SciVerse ScienceDirect

Renewable Energy

journal homepage: www.elsevier.com/locate/renene

Impedance-based diagnosis of polymer electrolyte membrane fuel cell failures associated with a low frequency ripple current

Jonghoon Kim [a,*], Inhae Lee [b], Yongsug Tak [b], B.H. Cho [a]

[a] Power Electronics System Laboratory, School of Electrical Engineering and Computer Science, Seoul National University, Seoul 151-744, Republic of Korea
[b] Materials and Electro-Chemistry Laboratory, Department of Chemical Engineering, Inha University, Incheon 402-751, Republic of Korea

ARTICLE INFO

Article history:
Received 5 September 2011
Accepted 26 September 2012
Available online 26 October 2012

Keywords:
Low frequency ripple current
Polymer electrolyte membrane fuel cell
Degradation
Cathode flooding
Membrane drying

ABSTRACT

This work deals with a diagnosis of cathode flooding and membrane drying associated with a low frequency ripple current of a polymer electrolyte membrane fuel cell (PEMFC) based on impedance measurement on 12 single cells using electrochemical impedance spectroscopy (EIS). Average values of the identified model parameters obtained from direct measurement of the impedance curves of 12 single cells obtained after cycling for hours at variable frequencies, it has been found that impedance magnitude of a fuel cell injecting a low frequency ripple current (100 Hz) increased when compared with those injecting high frequency ripple currents (1 kHz and 10 kHz). Based on these investigations, additional impedance measurements are directly conducted to gain insight into cathode flooding and membrane drying concerning a low frequency ripple current. Regardless of operating frequency of ripple current, two PEMFC failures lead to an increase in the impedance magnitude in comparison with that of a fresh cell. Specifically, it is shown that a low frequency ripple current more accelerates the PEMFC degradation associated with two PEMFC failures.

1. Introduction

Much attention has been paid to fuel cells because they offer a highly environmentally friendly technology for energy conversion. Of the various types of fuel cells available, polymer electrolyte membrane fuel cell (PEMFC) are considered to be the most promising energy technology with the advantages of low-operating temperature, high current density, high potential for low cost and volume, fast start-up ability, and suitability for discontinuous operation become the most promising and attractive candidate for electric vehicle power [1–3].

In general, the PEMFC stack output or the power conditioning system (PCS) input is a low direct current (DC) voltage with a wide variation range. Therefore, it is necessary to install a PCS between the fuel cell and load in order to convert the low DC voltage into an alternating current (AC) voltage (120/240 V, 60 Hz). As a result, in the field of power electronics, a large amount of work has been accomplished on the integration of PEMFCs into distributed generation technologies [4–7]. However, one of key difficulties of the PCS is the low frequency ripple current produced by the inverter, as shown in Fig. 1. It is expected that the low frequency ripple current will affect not only the fuel cell capacity, but also the fuel consumption and life span of the fuel cell [8–10]. Choi et al. indicated that a fuel cell needs a higher power handling capability in order to reduce the low frequency ripple current [11]. A ripple current of 100 Hz exhibits hysteresis behavior and injecting a ripple current that is around this frequency to a fuel cell may result in thermal problem among the stacks and impair the stack life expectancy [12]. Therefore, in order to reduce the low frequency ripple current that flows to a fuel cell, a PEMFC system requires a power conditioning by a DC–DC converter to mitigate ripple current and to achieve high efficiency, as shown in Fig. 2 [13–17]. In this perspective, a reduction of the low frequency ripple current is critical issue in practical applications where it is necessary to determine how long the fuel cell will last, and to minimize the risk of permanent internal damage.

One of the most important problems in PEMFC is the complex water management. In excess water condition, water vapor in the cells can condense and block the gas transport in the electrode, a gas diffusion layers (GDL) and gas channels. This can lead to unstable cell voltages PEMFC stacks are often operated at a current density below their maximum power point to avoid flooding and to keep the voltage stable. At low current densities and high temperatures, the cell membranes tend to dry out and their

* Corresponding author. Tel.: +82 2 880 1785; fax: +82 2 878 1452.
E-mail address: qwzxas@hanmail.net (J. Kim).

0960-1481/$ – see front matter © 2012 Elsevier Ltd. All rights reserved.
http://dx.doi.org/10.1016/j.renene.2012.09.053

Nomenclature

PEMFC	polymer electrolyte membrane fuel cell
PCS	power conditioning system
DC	direct current
AC	alternative current
GDL	gas diffusion layers
EIS	electrochemical impedance spectroscopy
MEA	membrane electrode assembly
R_Ω	membrane resistance (PEMFC model)
R_{ct}	charge transfer resistance (PEMFC model) (a): anode, (c): cathode
C_{dl}	double layer capacitance (PEMFC model) (a): anode, (c): cathode
Z_w	Warburg impedance (PEMFC model) (a): anode, (c): cathode
σ	ionic conductivity
τ	time constant
H_2, O_2, N_2	hydrogen, oxygen, nitrogen
F	Faraday's constant (96,439 C/mole)
M_{H_2}	hydrogen molar mass (2.016×10^{-3} kg/mol)
M_{O_2}	oxygen molar mass (32×10^{-3} kg/mol)
λH_2	hydrogen excess ratio
λO_2	oxygen excess ratio
W^{in}_{an,H_2}	hydrogen gas flow rate
W^{in}_{ca,O_2}	oxygen gas flow rate
W^{react}_{an,H_2}	hydrogen flow necessary for the reaction
W^{react}_{ca,O_2}	oxygen flow necessary for the reaction
ΔR_L	increased resistance due to the degradation (ripple current)
ΔC_{dlL}	decreased capacitance due to the degradation (ripple current)
τ_L	time constant (ripple current)
H^+	proton or a hydrogen ion
R_D	resistance due to the degradation (membrane drying)
R_F	resistance due to the degradation (cathode flooding)
ΔR	$(R_D + R_F)$ increased resistance due to the PEMFC failures
ΔC_{dlW}	decreased capacitance due to the PEMFC failures

protonic conductivity and mechanical stability decreases [18–24]. For the diagnosis of these PEMFC failures, it is necessary to have a good understanding of the PEMFC degradation but the lack of adequate tools for monitoring the degradation is a hurdle. Efficient control and supervision of the fuel cell system relies on creating a representation that describes the behavior of the cell appropriately. Therefore, electrochemical impedance spectroscopy (EIS) is established as a powerful characterization tool to detect different failure mechanisms occurring in a fuel cell. Impedance spectra can help to characterize a cell in much more sophisticated manner than just analyzing the polarization curve [25,26]. Merida et al. used this technique in order to investigate flooding and drying out issues in a four-cell stack [25]. The two failures could be separated by operating the impedance measurement in a separate frequency range. Roy et al. used impedance spectroscopy measurement and the stochastic character of the flooding for a robust diagnosis. Their work shows the potential of impedance error analysis methodology for drying out and flooding detection [26].

Great attention has been shown to the question of a low frequency ripple current. A great deal of research has been devoted to settling the problems of a low frequency ripple current [4–12]. Unfortunately, however, these studies have only been concerned with a fresh PEMFC. To date, there has been minimal research regarding the PEMFC failures associated with a low frequency ripple current. In addition, there is no experimental evaluation and comparison of the effects of high frequency and low frequency ripple currents through immediate measurement on a PEMFC single cell.

In this study, a diagnosis of cathode flooding and membrane drying associated with a low frequency ripple current of a PEMFC based on impedance measurement using EIS is presented. The obtained average values of the identified model parameters from direct measurement of the impedance curves of 12 single cells obtained cycling for hours at variable frequencies (100 Hz, 1 kHz, and 10 kHz) can help to explain that the low frequency ripple current (100 Hz) leads to the most marked difference in the diameter of the overlapping arc from that of a fresh cell. The present study develops these investigations one step further by showing impedance measurement on six single cells previously used during operation in flooding and drying modes concerning a low frequency ripple current. Regardless of operating frequency of ripple current, two PEMFC failures lead to an increase in the impedance magnitude when compared with that of a fresh cell. In particular, it is shown that impedance measurements under two specific frequencies ripple currents, one high (10 kHz) and one low frequency ripple current (100 Hz), are sufficient to present the effect that a low frequency ripple current more accelerates the PEMFC degradation associated with two PEMFC failures.

2. Typical impedance curve for a PEMFC

The EIS is a dynamic characterization technique in which a small AC perturbation signal (voltage in potentiostatic mode, current in galvanostatic mode) is applied to the system at variable frequencies. For each frequency, the magnitude and phase of the resulting signal that measures the impedance are determined [27–29].

Fig. 3 shows a typical Nyquist plot and the circuit that fits most of the PEMFC [29]. The processes that occur inside a fuel cell can be analyzed using the circuit elements of resistors and capacitors. The circuit elements describe the behavior of electrochemical reaction kinetics, the ohmic conduction processes, and mass transport using

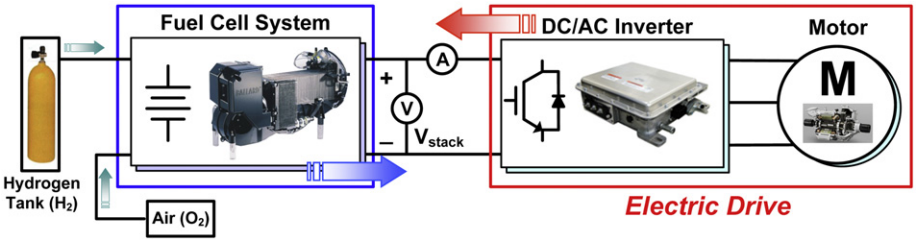

Fig. 1. Block diagram of power conditioning system (PCS) without DC–DC converter.

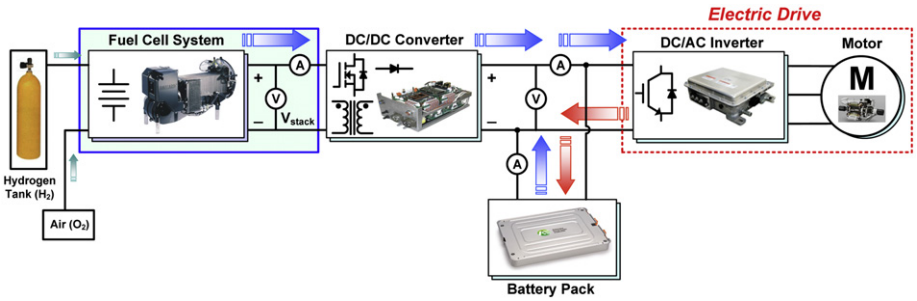

Fig. 2. Block diagram of power conditioning system (PCS) with DC–DC converter.

an impedance spectrum by EIS. At the highest frequencies measured, the impedance tends to the real axis at a resistance. As expressed in Eq. (1), the impedance of a resistor is represented as a single point on the real axis and is independent of frequency.

$$Z_R(\omega) = R_\Omega \tag{1}$$

where ω is the frequency of the AC signal. As expressed in Eq. (2), a resistor R_{ct} and capacitor C_{dl} in parallel represents the impedance behavior of an electrochemical reaction interface.

$$Z_{RC\_parallel}(\omega) = \frac{1}{R_{ct}^{-1} + j\omega C_{dl}} = \frac{R_{ct}}{1 + j\omega R_{ct} C_{dl}} = \frac{R_{ct}(1 - j\omega\tau)}{(1 + j\omega\tau)(1 - j\omega\tau)} = \frac{R_{ct}}{1 + \omega^2\tau^2} - j\frac{\omega\tau R_{ct}}{1 + \omega^2\tau^2} \tag{2}$$

where $\tau = R_{ct}C_{dl}$ is the time constant, which is considered a measure of the rate of a reaction or process. In the complex–plane diagram, the Nyquist plot of resistance and capacitance in parallel is an ideal semicircle. The diameter equals the value of the resistance, R_{ct}. The capacitance C_{dl} describes the charge separation across the interface. The imaginary part of the impedance reaches a maximum at frequency ω_{max}, denoted as the characteristic frequency. The charge transfer resistances in the anode and cathode are $R_{ct(a)}$ and $R_{ct(c)}$, respectively. The double layer capacitance in the anode is $C_{dl(a)}$ and that of the cathode is $C_{dl(c)}$. As shown in Fig. 3, the Nyquist plot shows two semicircles. The first loop corresponds to the RC model of the anode activation kinetics while the second loop corresponds to the RC model of the cathode activation kinetics. A Warburg resistance represents the resistance related to mass transfer in an electrochemical process. The resistance is frequency-dependent. The impedance of the Warburg resistance is written as follows.

$$Z_w(\omega) = \frac{\sigma}{\sqrt{\omega}}(1 - j) = \sigma\omega^{-\frac{1}{2}} - j\sigma\omega^{-\frac{1}{2}} \tag{3}$$

where σ is the ionic conductivity. The Warburg impedance can be considered as a resistance connected with a capacitance in series. Since the impedance of the real part equals that of the imaginary part, in Nyquist spectra the Warburg impedance is represented by the 45° line following the semicircle. $Z_{w(a)}$ and $Z_{w(c)}$ are the Warburg impedances associated with the gas diffusion in the anode and cathode, respectively.

3. Single cell test with a ripple currents at variable frequencies

3.1. Experimental setup

The experimental setup was designed for analyzing the applied ripple current with variable characteristic frequencies in a PEMFC that was directly made by the 'Materials and Electro-Chemistry Laboratory at Inha University' [30]. A block diagram of the setup is presented in Fig. 4. All experiments were conducted using 12 subscale single cells (with an active area of 25 cm^2). The membrane electrode assembly (MEA) that was used a GORE™ PRIMEA® SERIES 57 MEA (W. L. Gore & Associates, Inc.) which has 0.4 mg/cm^2 Pt on both the anode and the cathode. The GDLs were SIGRACET® GDL 10 BB (thickness of 420 μm, SGL Carbon Japan Ltd.). High purity H_2 (99.99%) gas for the anode feed, high purity Air (O_2 21%/N_2) for the cathode feed, and high purity N_2 (99.99%) gas for both the anode and cathode feed were used. These gases were humidified in a bubbling humidifier before entering the fuel cell. The temperature of the cell was 70 °C and the humidification temperature was 70 °C (100% RH). An average current of 20 A was applied during the experiments in order to examine the ripple current. As a consequence, only gas flow rates (H_2 and O_2) corresponding to 20 A were supplied: W^{in}_{an,H_2} and W^{in}_{ca,O_2}. In general, these gas flows need to be controlled rapidly and efficiently in order to avoid hydrogen/oxygen starvation and to extend the cell life. Moreover, these flows supplied to the anode and cathode should exceed the hydrogen/oxygen flows necessary for the reaction: W^{react}_{an,H_2} and W^{react}_{ca,O_2}. The hydrogen flow W^{react}_{an,H_2} and oxygen flow W^{react}_{ca,O_2} that react to produce a certain cell current I, are defined as Eqs. (4) and (5), respectively [30,31].

$$W^{react}_{an,H_2} = M_{H_2} \times \frac{I}{2F} \tag{4}$$

$$W^{react}_{ca,O_2} = M_{O_2} \times \frac{I}{4F} \tag{5}$$

where M_{H_2} and M_{O_2} are the hydrogen molar mass (2.016×10^{-3} kg/mol) and oxygen molar mass (32×10^{-3} kg/mol), respectively. This leads to hydrogen/oxygen excess ratios, λH_2 and λO_2, that are defined as the ratio of the supplied hydrogen/oxygen to the hydrogen/oxygen used in the anode and cathode, as expressed in Eqs. (6) and (7), respectively [30].

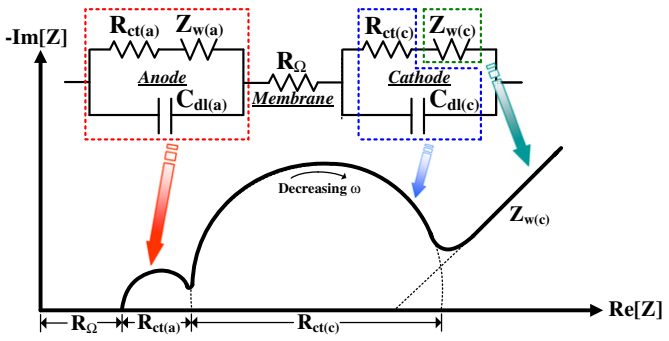

Fig. 3. Equivalent circuit model and corresponding Nyquist plot.

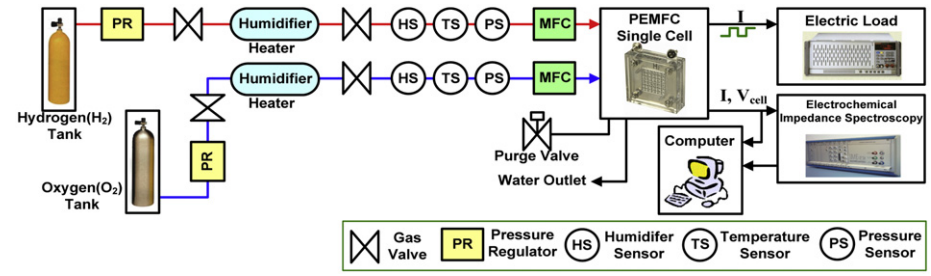

Fig. 4. Experimental setup for a single cell test.

$$\lambda H_2 = \frac{W^{in}_{an,H_2}}{W^{react}_{an,H_2}} \tag{6}$$

$$\lambda O_2 = \frac{W^{in}_{ca,O_2}}{W^{react}_{ca,O_2}} \tag{7}$$

These ratios must be restricted to $\lambda H_2 \geq 1.0$ and $\lambda O_2 \geq 1.2$, because under this limit, the fuel cell suffers hydrogen/oxygen starvation effects. This range is also close to the high efficiency range. In this study, the experiments were performed with H_2 and O_2 under the constant stoichiometry mode of $\lambda H_2 = 1.5$ and $\lambda O_2 \geq 2.0$. In the case of H_2, a mass flow rate W^{in}_{an,H_2} within 30 A can be used to avoid hydrogen starvation. In the case of O_2, a mass flow rate W^{in}_{ca,O_2} within 40 A can be used. However, due to the slow diffusion of oxygen, a mass flow rate within 33.3 A (40/1.2) should be used. Consequently, it is necessary to determine the maximum hydrogen/oxygen excess ratios to avoid hydrogen/oxygen starvation. The gas flow rates corresponding to a stoichiometry of 1.5 and 2 for H_2 and air are 209 ppm (209 mg/kg) and 668 ppm (668 mg/kg), respectively. A square wave ripple current (average 20 A, peak-to-peak 10–30 A), shown in Fig. 5, was applied to the 12 PEMFC single cells at three frequencies (100 Hz, 1 kHz, and 10 kHz) for 100 h. Under experimental condition at a specific frequency, a square wave ripple current was applied to three single cells. Therefore, a total of 12 single cells were used to measure the identified model parameters via AC impedance measurement at all operating frequency range. For reference, due to the limitation of the experimental apparatus (electric load), a sinusoidal wave ripple current could not be applied to the PEMFC. Each impedance curve was obtained after 100 h and compared using the EIS. The impedance measurement was conducted at steady-state condition in galvanostatic mode for frequency range of 2 kHz–0.03 Hz, with 51 measurement points and ±1 mA amplitude (Zahner, IM6ex). Inductive behavior from the wires was predominant above 2 kHz, while the instability of the system led to highly irreproducible results below 0.03 Hz.

3.2. Experimental results

The Nyquist plots of the experimental fuel cell impedance measurement obtained with the application of variable frequencies

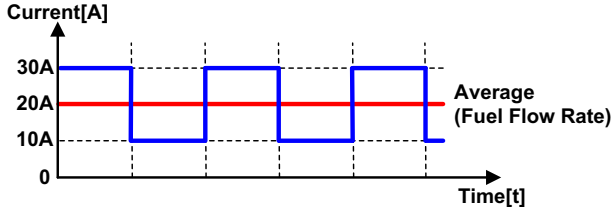

Fig. 5. Square wave ripple current (average 20 A, peak-to-peak 10 ~ 30 A).

ripple currents for 100 h are shown in Fig. 6. The low frequency ripple current leads to the largest difference in the diameter of the overlapping arc compared to that of a fresh cell. At a low frequency of 100 Hz, where inverters produce more ripples (120 Hz), fuel cell degradation can be more pronounced.

To better understand the electrochemical processes involved in the operation of the fuel cell, in accordance with the characteristics of fuel cell reaction and our measured impedance spectra, a basic equivalent circuit shown in Fig. 3 has been setup. Among the total ohmic losses represented by R_Ω, it is known that the ohmic resistance is the most significant internal loss. In a Nyquist plot, the intercept of the high frequency with the real axis represents the total ohmic resistance R_Ω. In general, for H_2–O_2 fuel cells, the electrochemical reaction rate at the cathode is slow compared to that of the anode. The oxygen reduction in the cathode is considerably slower than the hydrogen oxidation reaction. Due to the faster rate of the anode activation reaction [32,33], the double layer capacitance $C_{dl(a)}$ and charge transfer resistance $R_{ct(a)}$ at the anode are captured at higher frequencies (from 2 kHz to 60 Hz). $C_{dl(c)}$ and $R_{ct(c)}$ at the cathode are captured at comparatively lower frequencies from 60 Hz to 0.03 Hz. Thus, activation losses at the cathode dominate over those of the anode. As the cathode impedance are merges, the effective fuel cell charge transfer resistance is assumed to be $R_{ct(c)} \approx R_{ct}$, as expressed in Eq. (8).

$$Z(\omega) = R_\Omega + \frac{1}{\dfrac{1}{R_{ct} + \dfrac{\sigma}{\sqrt{\omega}}(1-j)} + j\omega C_{dl}} \tag{8}$$

The Warburg impedance Z_w employed to represent and evaluate the low frequency diffusive effects in our experimental fuel cell has

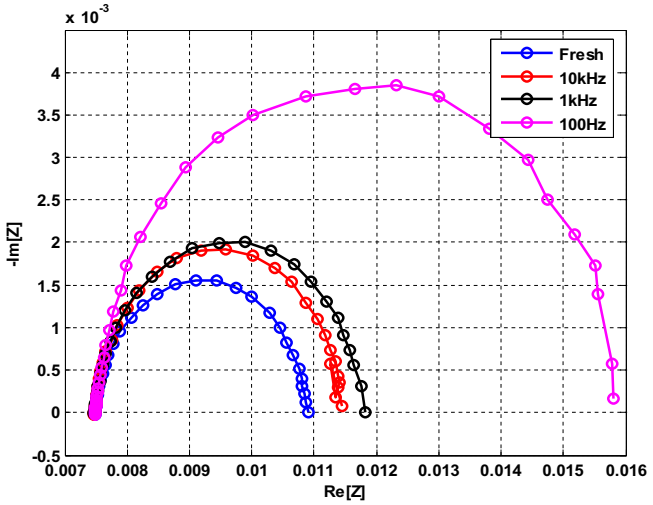

Fig. 6. Impedance curves on single cells obtained after cycling for 100 h at variable frequencies (100 Hz, 1 kHz, and 10 kHz).

not been recognized. This impedance is ignored at extremely low frequencies (<0.03 Hz). Therefore, as shown in Fig. 7(a), the simplified model of an electrochemical interface can be built. The total impedance can be calculated by

$$Z(\omega) = R_{\Omega} + \frac{1}{\frac{1}{R_{\mathrm{ct}}} + j\omega C_{\mathrm{dl}}} = R_{\Omega} + \frac{R_{\mathrm{ct}}}{1+\omega^2\tau^2} - j\frac{\omega\tau R_{\mathrm{ct}}}{1+\omega^2\tau^2} \quad (9)$$

where $\tau = R_{\mathrm{ct}}C_{dl}$ is the time constant, which is considered a measure of the rate of a reaction or process. The product $R_{\mathrm{ct}}C_{dl}$ controls the distribution of the total current between the charging of the double layer and the electrochemical reaction. The Nyquist plot of this model is always a semicircle. At high frequencies, the impedance of C_{dl} is very low, so the measured impedance tends to R_{Ω}. At low frequencies, the impedance of C_{dl} becomes extremely high, and thus, the measured impedance tends to $R_{\Omega} + R_{\mathrm{ct}}$. Accordingly, at intermediate frequencies, the impedance falls between R_{Ω} and $R_{\Omega} + R_{\mathrm{ct}}$. The high frequency intercept is associated with the ohmic resistance, while the low frequency intercept corresponds to the sum of the ohmic resistance and the charge transfer resistance. The diameter of the semicircle is equal to the charge transfer resistance. Therefore, the outcome of the experiment shown in Fig. 6 can be expressed in Eq. (10). The impedance can be recalculated by

$$\begin{aligned} Z(\omega) &= R_{\Omega} + \frac{1}{\frac{1}{R_{\mathrm{ct}}+\Delta R_L} + j\omega(C_{\mathrm{dl}} + \Delta C_{\mathrm{dl}L})} \\ &= R_{\Omega} + \frac{R_{\mathrm{ct}}+\Delta R_L}{1+\omega^2\tau_L^2} - j\frac{\omega\tau_L(R_{\mathrm{ct}}+\Delta R_L)}{1+\omega^2\tau_L^2} \end{aligned} \quad (10)$$

where ΔR_L is the increased resistance and $\Delta C_{\mathrm{dl}L}$ is the decreased capacitance due to the degradation associated with a low frequency ripple current, respectively. In addition, $\tau_L = (R_{\mathrm{ct}} + \Delta R_L)(C_{\mathrm{dl}} + \Delta C_{\mathrm{dl}L})$ is the time constant. As shown in Fig. 6, the low frequency ripple current has a significant effect on the AC impedance. Based on the simplified equivalent circuit model shown in Fig. 7(b), average values of the identified model parameters on 12 single cells injecting ripple currents at variable frequencies are presented in Table 1, with the assumption of identical time constant τ_L [30].

4. PEMFC failures associated with a low frequency ripple current

4.1. PEMFC failures

Fuel cells have challenging problems associated with their durability and life expectancy. Many researchers have reported a decrease in the cell voltage performance with an increase in the effects of membrane drying and cathode flooding [18–24].

The membrane of a PEMFC has to be wet for normal operation. As shown in Fig. 8, the water inside the membrane transports protons (H^+) from the anode to the cathode by osmosis. A sufficient amount of water in the membrane is achieved by humidifying the incoming hydrogen (H_2) and oxygen (O_2). However, improper operating temperatures, air flow rates, and humidity can lead to too little or too much water being injected into the fuel cell, which, in turn, causes membrane drying or cathode flooding, respectively. Prolonged operation during these two states decreases the output power of the fuel cell. For membrane drying to occur, insufficient water is injected into the cell causing it to operate at a low current density. As the membrane of the cell dries out, the voltage gradually drops. Eventually, the cell dries out and the voltage drops suddenly to zero in a similar manner to a concentration drop.

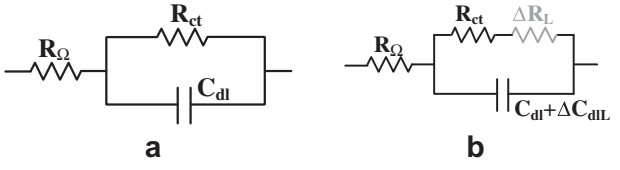

Fig. 7. Simplified equivalent circuit models. (a) No injecting a low frequency ripple current, (b) Injecting a low frequency ripple current.

Table 1
Average values of the identified model parameters on 12 single cells injecting ripple currents at variable frequencies (100 Hz, 1 kHz and 10 kHz) based on impedance curves.

	Fresh	10 kHz	1 kHz	100 Hz
R_{Ω} [Ω]	0.00745	0.00756	0.00770	0.00790
R_{ct} [Ω]	0.00345	0.00355	0.00368	0.00387
ΔR_L [Ω]	0	0.00034	0.00044	0.00403
$C_{dl} + \Delta C_{\mathrm{dl}L}$ [F]	1.08032	0.95812	0.90463	0.47178

An excess of water leads to a decrease of active surface by flooding a part of the pores of the cathode. As the active surface decreases the remaining surface is operated in the galvanostatic mode of operation at higher current densities and thus at higher overvoltage and lower cell voltage, respectively. The accumulation of liquid water inside the cathode GDL of the cell is a slow process. During this process, the voltage drops slowly as if the current was limited by the diffusion of the reactants. Eventually, water droplets are formed inside the gas channels which prevent oxygen from reaching the catalytic sites, thus rapidly reducing the cell voltage to zero.

In a PEMFC, the conductivity of the PEMFC is directly related to its water content [19]. Membrane drying of the membrane lead to an increase of membrane resistance and a decrease of PEMFC output power. Insufficient humidification may result in very poor oxygen electroctalysis and in increased resistance in catalyst layers. An excess of water in the cathode lead to condensation and subsequent flooding. Flooding increases the resistance associated with the GDL and may even block flow channels, reducing the availability of oxygen [26]. On the basic process of two PEMFC failures, two resistances that represent PEMFC failures due to membrane drying (R_D) and cathode flooding (R_F) are defined in this work, respectively.

4.2. Experimental results for PEMFC failures associated with a low frequency ripple current

It has been found that impedance magnitude of a fuel cell injecting a low frequency ripple current (100 Hz) increased when compared with those injecting high frequency ripple currents (1 kHz and 10 kHz). In Section 4.2, the present study develops these investigations one step further by showing impedance measurement on six single cells during operation in flooding and drying modes concerning a low frequency ripple current. With two specific frequencies ripple currents, one high (10 kHz) and one low frequency ripple current (100 Hz), we measured the membrane drying and cathode flooding in fuel cells under load using EIS.

Under experimental condition at a specific frequency, a square wave ripple current was applied to six single cells previously used including three cells at high frequency (10 kHz) and the other three cells at low frequency (100 Hz) among 12 cells. The normal case,

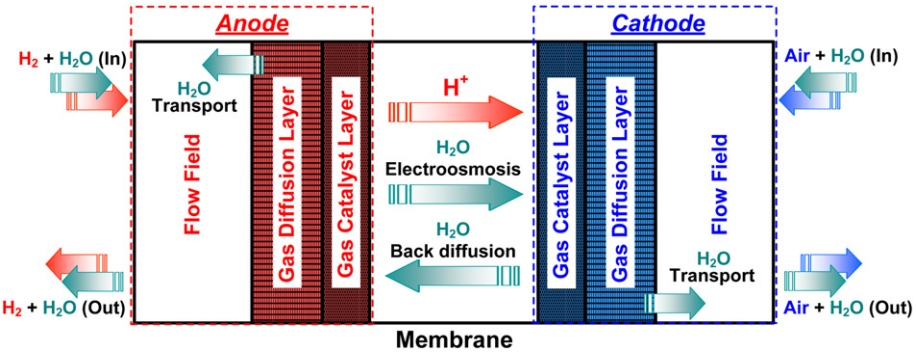

Fig. 8. Schematic picture of water movement inside a PEMFC.

flooding and drying have each been experimented with under different operating conditions. Fig. 9 shows the voltages of the cell (anode and cathode) affected by a low frequency ripple current (100 Hz) during a 7.5 h long experiment in which the cell was successively operated in normal, flooded, and dry conditions. The DC current was kept constant for the whole duration of the test, so as to ensure the state-of-health (SOH) [34–36] of the fuel cell is solely responsible for the voltage variation. The cathode inlet gas relative humidity was kept at 50% or 100% to avoid membrane drying and cathode flooding under normal conditions. In addition, the cell and humidifier temperatures were initially kept the same for normal operation. The temperature of the cell and the humidifier are 70 °C. Degradation in the cell operation can easily be detected by measuring the cell voltage. As the cathode inlet relative humidity increases to an excessive humidity level (120%), the flooding process leads to a drop in the cell voltage. On the other hand, as the cathode inlet relative humidity decreases to a zero humidity level (0%), the drying process leads to a drop in the cell voltage.

The three spectra of the cells affected by high and low frequency ripple currents during normal, flooded, and dry conditions are shown in Fig. 10. Fig. 10(a) shows the impedance spectra on three single cells with a high frequency ripple current (10 kHz). In addition, the impedance spectra on three single cells with a low frequency ripple current (100 Hz) are shown in Fig. 10(b). The interception of the high frequency impedance loop with the real axis changes only a little with normal, flooded, and dry conditions. However, both the real and imaginary parts of the cell impedance during flooded and dry conditions increase compared with the results under normal conditions. In the case of a flooded fuel cell, both the real and imaginary parts of the impedance grow larger than those of a dry fuel cell. Experimental results show the similar shape (semicircle) of the impedance curves, as seen in Fig. 10. It appears clearly that the processes of drying and flooding are characterized by the modification of the low frequency part (an increase in the charge transfer resistance) of the fuel cell impedance, which, in turn, is associated with the low frequency ripple current. It is clearly seen that the low frequency ripple current causes the largest difference in the diameter of the overlapping arc compared with three spectra of the cell affected by the high frequency ripple current.

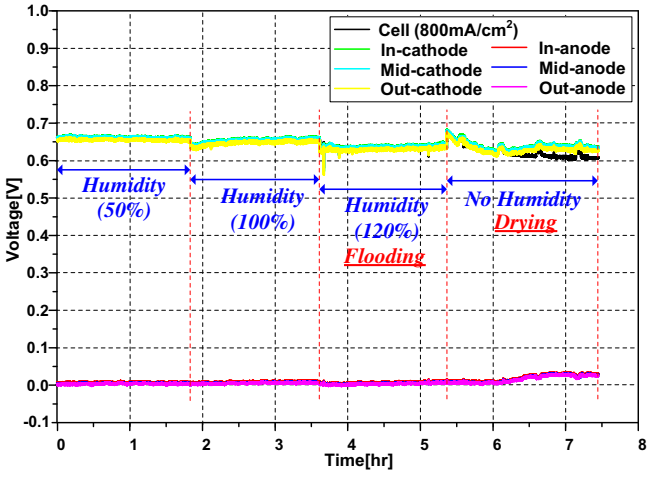

Fig. 9. Cell voltage of a fuel cell in flooded, normal, and dry condition.

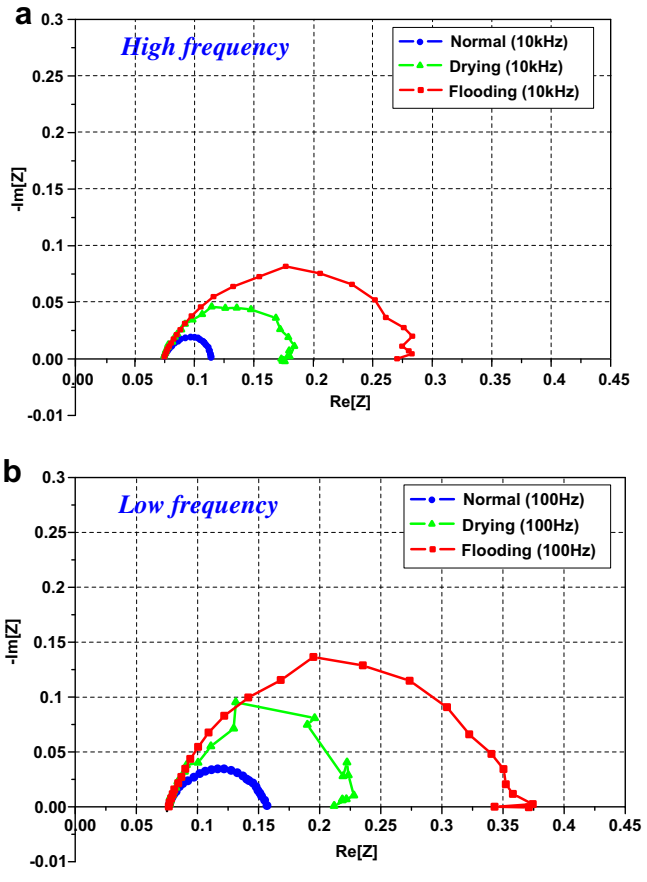

Fig. 10. Impedance spectra on single cells injecting ripple currents in flooded, normal, and dry condition at two specific frequencies. (a) 10 kHz, (b) 100 Hz.

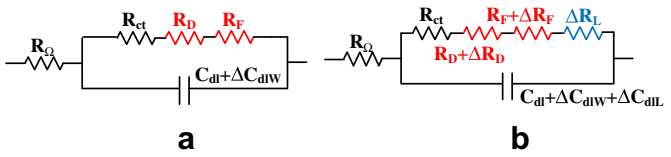

Fig. 11. Simplified equivalent circuit models in flooded and dry condition (a) No injecting a low frequency ripple current, (b) Injecting a low frequency ripple current.

As mentioned earlier, the increase in the charge transfer resistance causes the increase in the diameter of the cell impedance response with a low frequency ripple current. As shown in Fig. 7, an increased resistance ΔR_L and a decreased capacitance ΔC_{dlL} associated with a low frequency ripple current were identified in Section 3.2. In the same manner, membrane drying and cathode flooding lead to an increase in the charge transfer resistance with a low frequency ripple current. Consequently, as shown in Fig. 11, two resistances R_D and R_F with different values associated with the PEMFC failures are more varied by low frequency ripple current and can be added in the cathode of the model shown in Fig. 7.

The increase in the value of the resistance R_F is a significant marker of cathode flooding only. On the other hand, the parameter R_D is not affected by cathode flooding but by membrane drying. The total impedance considering PEMFC failures can be calculated by

$$\begin{aligned} Z(\omega) &= R_\Omega + \frac{1}{\dfrac{1}{R_{ct}+R_D+R_F} + j\omega(C_{dl}+\Delta C_{dlW})} \\ &= R_\Omega + \frac{R_{ct}+\Delta R}{1+\omega^2\tau_w^2} - j\frac{\omega\tau_w(R_{ct}+\Delta R)}{1+\omega^2\tau_w^2} \end{aligned} \tag{11}$$

where $\Delta R = R_D + R_F$ is the increased resistance and ΔC_{dlW} is the decreased capacitance associated with the PEMFC failures, respectively. With ΔR_L and ΔC_{dlL} associated with the low frequency ripple current, the total impedance can be recalculated by

$$\begin{aligned} Z(\omega) &= R_\Omega + \frac{1}{\dfrac{1}{R_{ct}+\Delta R+\Delta R_L} + j\omega(C_{dl}+\Delta C_{dlL})} \\ &= R_\Omega + \frac{R_{ct}+\Delta R+\Delta R_L}{1+\omega^2\tau_{all}^2} - j\frac{\omega\tau_{all}(R_{ct}+\Delta R+\Delta R_L)}{1+\omega^2\tau_{all}^2} \end{aligned} \tag{12}$$

$\tau_{all} = (R_{ct}+\Delta R+\Delta R_L)(C_{dl}+\Delta C_{dlW}+\Delta C_{dlL})$ is the time constant. As shown in Fig. 11, the low frequency ripple current has a significant effect on the AC impedance of a fuel cell degraded by flooding and drying. Based on simplified equivalent circuit model shown in Fig. 11, average values of the identified model parameters on six single cells injecting ripple currents at two frequencies (10 kHz and 100 Hz) are listed in Tables 2 and 3, respectively, with the assumption of identical time constant τ_{all}. As shown in Tables 2 and 3, the variation of the model parameters while the membrane is drying is less than in the case of the flooding.

Table 2
Average values of the identified model parameters on three single cells injecting a high frequency ripple current (10 kHz) in flooded, normal, and dry conditions based on impedance curves.

	R_Ω [Ω]	R_{ct} [Ω]	ΔR_L [Ω]	R_D [Ω]	R_F [Ω]	$C_{dl}+\Delta C_{dlW}+\Delta C_{dlL}$ [F]
Normal	0.00756	0.00355	0.00034	0	0	0.95812
Drying	0.00763	0.00366	0.00037	0.16355	0	0.02152
Flooding	0.00767	0.00373	0.00044	0	0.26083	0.01367

Table 3
Average values of the identified model parameters on three single cells injecting a low frequency ripple current (100 Hz) in flooded, normal and, dry conditions based on impedance curves.

	R_Ω [Ω]	R_{ct} [Ω]	ΔR_L [Ω]	R_D [Ω]	R_F [Ω]	$C_{dl}+\Delta C_{dlW}+\Delta C_{dlL}$ [F]
Normal	0.00790	0.00387	0.00403	0	0	0.47178
Drying	0.00796	0.00396	0.00412	0.19772	0	0.01743
Flooding	0.00805	0.00402	0.00418	0	0.32486	0.01147

5. Conclusion

Based on impedance measurement on single cells using EIS, a diagnosis of two PEMFC failures (cathode flooding, membrane drying) associated with a low frequency ripple current is presented in this study. Through the direct measurement of the impedance curves of 12 single cells obtained after cycling for hours at variable frequencies, it has been found that impedance magnitude of a fuel cell injecting a low frequency ripple current (100 Hz) increased when compared with those injecting high frequency ripple currents (1 kHz and 10 kHz). The study develops these investigations one step further by showing impedance measurement on single cells during operation in flooding and drying modes concerning a low frequency ripple current. Regardless of operating frequency of ripple current, two PEMFC failures lead to an increase in the impedance magnitude when compared with that of a fresh cell. In particular, it is shown that impedance measurements under two specific frequencies ripple currents, one high (10 kHz) and one low frequency ripple current (100 Hz), are sufficient to present the effect that a low frequency ripple current more accelerates the cell degradation associated with two PEMFC failures.

Acknowledgments

This work was supported by the New and Renewable Energy Program of the Korea Institute of Energy Technology Evaluation and Planning (KETEP) grant funded by the Korea government Ministry of Knowledge Economy (No. 20104010100490).

References

[1] Corbo P, Migliardini F, Veneri O. PEFC stacks as power sources for hybrid propulsion systems. Int J Hydrog Energy 2009;34:4635–44.
[2] Hernandez A, Hissel D, Outbib R. Modeling and fault diagnosis of a polymer electrolyte fuel cell using electrical equivalent analysis. IEEE Trans Energy Convers 2010;25(1):148–60.
[3] Wu S-J, Shiah S-W, Yu W-L. Parametric analysis of proton exchange membrane fuel cell performance by using the Taguchi method and a neural network. Renew Energ 2009;34:135–44.
[4] Giustiniani A, Petrone G, Spagnuolo G, Vitelli M. Low-frequency current oscillations and maximum power point tracking in grid-connected fuel-cell-based systems. IEEE Trans Ind Electron 2010;57(6):2042–53.
[5] Fontes G, Turpin C, Astier S, Meynard TA. Interactions between fuel cells and power converters: influence of current harmonics on a fuel cell stack. IEEE Trans Power Electron 2007;22(2):670–8.
[6] Kovacevic G, Tenconi A, Bojoi R. Advanced DC–DC converter for power conditioning in hydrogen fuel cell systems. Int J Hydrog Energy 2008;33:3215–9.
[7] Hinaje M, Sadli I, Martin J-P, Thounthong P, Raël S, Davat B. Online humidification diagnosis of a PEMFC using a static DC–DC converter. Int J Hydrog Energy 2009;34:2718–23.
[8] Brey JJ, Bordallo CR, Carrasco JM, Galván E, Jimenez A, Moreno E. Power conditioning of fuel cell systems in portable applications. Int J Hydrog Energy 2007;32:1559–66.
[9] Olsen Berenguer FA, Molina MG. Design of improved fuel cell controller for distributed generation systems. IEEE Trans Int J Hydrog Energy 2010;35:5974–80.
[10] Kim J-S, Choe G-Y, Kang H-S, Lee B-K. Robust low frequency current ripple elimination algorithm for grid-connected fuel cell systems with power balancing technique. Renew Energ 2011;36:1392–400.

[11] Choi W-J, Howze JW, Enjeti P. Development of an equivalent circuit model of a fuel cell to evaluate the effects of inverter ripple current. J Power Sources 2006;158:1324–32.
[12] Fontes G, Turpin C, Saisset R, Meynard T, Astier S. Interactions between fuel cells and power converters influence of current harmonics on a fuel cell stack. In: IEEE power electronics specialist conference; 2004. p. 4729–35.
[13] Liu C, Lai J-S. Low frequency current ripple reduction technique with active control in a fuel cell power system with inverter load. IEEE Trans Power Electron 2007;22(4):1429–36.
[14] Mazumder SK, Burra RK, Acharya K. A ripple-mitigating and energy-efficient fuel cell power-conditioning system. IEEE Trans Power Electron 2007;22(4): 1437–52.
[15] Kwon J-M, Kim E-H, Kwon B-H, Nam K-H. High-efficiency fuel cell power conditioning system with input current ripple reduction. IEEE Trans Ind Electron 2009;56(3):826–34.
[16] Lee S-H, An T-P, Cha H. Mitigation of low frequency AC ripple in single-phase photovoltaic power conditioning systems. J Power Electron 2010;10(3):328–33.
[17] Leu C-S, Li M-H. A novel current-fed boost converter with ripple reduction for high-voltage conversion applications. IEEE Trans Ind Electron 2010;57(6): 2018–23.
[18] Steiner NY, Hissel D, Moçotéguy Ph, Candusso D. Diagnosis of polymer electrolyte fuel cells failure modes (flooding & drying out) by neural network modeling. Int J Hydrog Energy 2011;36:3067–75.
[19] Le Canut JM, Latham R, Mérida W, Harrington DA. Impedance study of membrane dehydration and compression in proton exchange membrane fuel cells. J Power Sources 2009;192:457–66.
[20] Mckay DA, Siegel JB, Ott W, Stefanopoulou AG. Parameterization and prediction of temporal fuel cell voltage behavior during flooding and drying conditions. J Power Sources 2008;178:207–22.
[21] Gerteisen D, Heilmann T, Ziegler C. Modeling the phenomena of dehydration and flooding of a polymer electrolyte membrane fuel cell. J Power Sources 2009;187:165–81.
[22] Le Canut J-M, Abouatallah RM, Harrington DA. Detection of membrane drying, fuel cell flooding, and anode catalyst poisoning on PEMFC stacks by electrochemical impedance spectroscopy. J Electrochem Soc 2006;153(5):A857–64.
[23] Gebregergis A, Pillay P, Rengaswamy R. PEMFC fault diagnosis, modeling, and mitigation. IEEE Trans Ind Appl 2010;46(1):295–303.
[24] Pozio A, Cemmi A, Mura F, Masci A, Serra E. Long-term durability study of perfluoropolymer membranes in low humidification conditions. J Solid State Electrochem 2011;15:1209–16.
[25] Mérida W, Harrington DA, Le Canut J-M, McLean G. Characterization of proton exchange membrane fuel cell (PEMFC) failures via electrochemical impedance spectroscopy. J Power Sources 2006;161:264–74.
[26] Roy SK, Orazem ME. Analysis of flooding as a stochastic process in polymer electrolyte membrane (PEM) fuel cells by impedance techniques. J Power Sources 2008;184:212–9.
[27] Puranik SV, Keyhani A, Khorrami F. State-space modeling of proton exchange membrane fuel cell. IEEE Trans Energy Convers 2010;25(3):804–13.
[28] Fouquet N, Doulet C, Nouillant C, Dauphin-Tanguy G, Ould-Bouamama B. Model based PEM fuel cell state-of-health monitoring via ac impedance measurement. J Power Sources 2006;159:905–13.
[29] O'Hayre R, Cha S-W, Colella W, Prinz FB. Fuel cell fundamentals. 1st ed. New York: MA: John Wiley & Sons; 2006.
[30] Kim J-H, Jang M-H, Choe J-S, Kim D-Y, Tak Y-S, Cho B-H. An experimental analysis of the ripple current applied variable frequency characteristic in a polymer electrolyte membrane fuel cell. J Power Electron 2011;11(1): 82–9.
[31] Ramos-Paja CA, Bordons C, Romero A, Giral R, Martínez-Salamero L. Minimum fuel consumption strategy for PEM fuel cells. IEEE Trans Ind Electron 2009; 56(3):685–96.
[32] Andreasen SJ, Jespersen JL, Schaltz E, Kær SK. Characterisation and modelling of a high temperature PEM fuel cell stack using electrochemical impedance spectroscopy. Fuel Cells 2009;4:463–73.
[33] Hsuen H-K. Performance equations of polymer electrolyte fuel cells. J Power Sources 2004;126:46–57.
[34] Kurz T, Hakenjos A, Krämer J, Zedda M, Agert C. An impedance-based predictive control strategy for the state-of-health of PEM fuel cell stacks. J Power Sources 2008;180:742–7.
[35] Onanena R, Oukhellou L, Candusso D, Harel F, Hissel D, Aknin P. Fuel cells static dynamic characterizations as tools for the estimation of their ageing time. Int J Hydrog Energy 2011;36:1730–9.
[36] Onanena R, Oukhellou L, Candusso D, Same A, Hissel D, Aknin P. Estimation of fuel cell operating time for predictive maintenance strategies. Int J Hydrog Energy 2010;35:8022–9.